Polaritonic excitations and Bose-Einstein condensation in the Rabi lattice model

Gaoke Hu,[1] Zhiguo Lü,[2] Haiqing Lin,[1] and Hang Zheng[2,*]
[1]*Beijing Computational Science Research Center, Beijing 100193, China*
[2]*Key Laboratory of Artificial Structures and Quantum Control (Ministry of Education), School of Physics and Astronomy, Shanghai Jiao Tong University, Shanghai 200240, China*

(Received 15 September 2021; revised 12 January 2022; accepted 23 March 2022; published 12 April 2022)

The unitary transformation method is used to study the properties of the polaritonic states and Bose-Einstein condensation in the Rabi lattice model, where the on-site two-level systems (TLSs) are coupled with the intersite hopping photons. It is shown that the counter-rotating coupling (CRC) between TLS and photon, which breaks down the conservation of the excitation numbers, may induce a long-range Ising-like interaction among intersite TLSs. We have shown that the coupled TLSs and photons are hybridized to form the polaritonic states, and the corresponding ground state and polaritonic excitation spectra are calculated by diagonalizing our transformed Hamiltonian. When the photon hopping J is weak, the excitation spectrum is gapped. But the gap decreases with increasing J, and at critical value $J = J_c$ the gap becomes zero at the Γ point and the ground state becomes instable. Thus, J_c is the phase transition point where the polaritons are condensed at the Γ point to form the delocalized superradiant phase. The results show that the larger detuning between TLS and photon favors the disorder insulator phase, which requires the stronger J_c to get the long-range order phase. The phase diagram of the delocalized superradiant phase transition has been obtained where there are no Mott lobes since the CRC breaks down the number conservation. The ground state and the excitation spectra of the delocalized superradiant phase are also calculated. It is shown that in the delocalized superradiant state the order parameter is the nonzero ground-state average of the photon annihilation operator. The polaritonic excitation has a finite excitation gap because the CRC breaks down the number conservation but leaves only a discrete symmetry, the parity conservation.

DOI: 10.1103/PhysRevA.105.043710

I. INTRODUCTION

The quantum Rabi model is a milestone to depict the basic light-matter interaction processes in nature with the applications in quantum optics, the cold-atom systems and strongly correlated systems. It describes a two-level system (TLS) coupled coherently with a bosonic cavity field [1]. Despite the simplicity of the Rabi model, it presents a rich variety of interesting phenomena, such as the Josephson junction [2] and the Bloch-Siegert shift [3]. The Hamiltonian $\hat{H}^R$ of the Rabi model reads

$$\hat{H}^R = \epsilon\hat{\sigma}^+\hat{\sigma}^- + \omega\hat{b}^\dagger\hat{b} + g\hat{\sigma}^x(\hat{b}^\dagger + \hat{b}), \tag{1}$$

where the TLS is represented by the Pauli matrices $\hat{\sigma}^\pm$, with the atom-photon coupling g, and $\hat{b}_i^\dagger(\hat{b}_i)$ is the creation (annihilation) operator of the single-mode cavity with the frequency ω. The counter-rotating coupling (CRC) terms in the Rabi model are given by

$$\hat{H}^{\mathrm{CRC}} = g(\hat{\sigma}^+\hat{b}^\dagger + \hat{\sigma}^-\hat{b}). \tag{2}$$

It is well known that the Rabi model is reduced to the Jaynes-Cummings (JC) model [4] by the rotating-wave approximation (RWA), i.e., the neglect of the CRC terms, when the coupling between the TLS and photon is relatively weak. Due to the conservation of the polariton number $\hat{N} = \hat{b}^\dagger\hat{b} + \hat{\sigma}^+\hat{\sigma}^-$, the JC model is solvable. When the coupling between photons and TLSs is comparable or larger than all decoherence rates, the system can be regarded in the strong-coupling regime. In this regime, the JC model can describe several experiments such as the vacuum Rabi oscillations in Rydberg atoms [5]. The achievements in circuit quantum electrodynamics allow realizing the ultrastrong-coupling (USC) regime [6,7], where the rate between the coupling strength and photon frequency reaches $g/\omega \gtrsim 0.1$. In the USC regime, the RWA is not valid anymore, and the counter-rotating terms would inevitably be expressed and lead to novel features [3]. Moreover, the photonic analog simulator of the quantum Rabi model is realized in the deep strong-coupling regime [8,9], where the rate reaches $g/\omega \gtrsim 1$.

In an experiment of trapped ions or ultracold atoms, the Rabi systems can couple together by tunneling of photons to form the Rabi lattice model (RLM). Recently, Mei *et al.* report an experimental realization of the Rabi-Hubbard model using trapped ions and present a controlled study of its equilibrium properties and quantum dynamics [10], where the Rabi-Hubbard model has the same Hamiltonian as the RLM we studied here, except for the long-range hopping decaying inverse cubically with the distance. With the relatively large distance between the cavities, the quantum optical systems allow for a high level of measurement and manipulation of individual cavities at the quantum level [11–14]. Therefore, the RLM can serve as a quantum simulator to understand the emergent phenomena in strongly interacting

*Email address: hzheng@sjtu.edu.cn

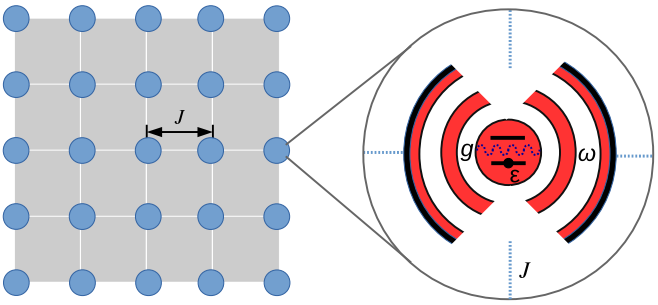

FIG. 1. Schematic of the Rabi lattice model in a two-dimensional square lattice. In each site, there is a cavity with the photon hopping strength J between the nearest-neighbor cavity. Each cavity is coupled with a two-level system.

condensed-matter systems [8,15–21]. The RLM involves two characteristic energy scales, the TLS energy split ϵ and the photon frequency ω, which provide an additional experimentally accessible detuning parameter $\Delta = \epsilon - \omega$. The two-component nature also furnishes rich physics, where the inherently combined photonic-atomic excitations enter entangled quantum states [22–24]. The composite nature of the polariton motivates us to build an effective polariton picture to understand all the unique features in the RLM. A theoretical method to illustrate the polaritonic excitation behavior is required.

The RLM is described by the Hamiltonian $\hat{H}$:

$$\hat{H} = \sum_i \hat{H}_i^R - J \sum_{\langle i,j \rangle} (\hat{b}_i^\dagger \hat{b}_j + \hat{b}_j^\dagger \hat{b}_i), \tag{3}$$

with the hopping strength J between nearest-neighbor cavities with i and j. A schematic of the RLM is shown in Fig. 1. Due to the phenomenon of photon blockade [25,26], the atom-photon coupling leads to an effective repulsion between photons. Under the RWA, the RLM reduces to the JC lattice model (JCLM), and the system undergoes a quantum transition from Mott insulator to superfluid phase [16,27]. In the insulator phase, the polaritons localize on each site, while the polaritons delocalize across the lattice to form a Bose-Einstein condensate in the superfluid phase. The important feature in RWA is the conservation of the polariton number. The JCLM is invariant under the generalized rotation operator, $\hat{R}(\theta) = \prod_i^N \exp[i\theta(\hat{b}_i^\dagger \hat{b}_i + \hat{\sigma}_i^+ \hat{\sigma}_i^-)]$, which means it exhibits continuous global $U(1)$ symmetry. Akin to the Bose-Hubbard systems, the phase diagram exhibits a similar lobe structure, which is confirmed by both numerical and analytical methods [16,22,23,27]. Low-lying hole and particle polaritonic excitations are explored beyond the mean-field approximation [22–24,28,29].

Although the RLM shares some properties with the JCLM, the remarkable qualitative difference in RLM is the CRC term breaks the conservation of the polariton number and reduces the symmetry from $U(1)$ to discrete global Z_2 symmetry [30,31], with the parity operator $\hat{P} = \prod_i^N \exp[i\pi(\hat{b}_i^\dagger \hat{b}_i + \hat{\sigma}_i^+ \hat{\sigma}_i^-)]$. The different properties of symmetry between RLM and JCLM consequently change the phase diagram and the polaritonic excitation behavior. In the JCLM, the state that breaks the $U(1)$ symmetry has a nonzero superfluid density, and the delocalized phase is characterized as the superfluid phase [16,27]. While the CRC terms in the RLM leave the system with a discrete Z_2 symmetry, the superfluid phase is replaced by the delocalized superradiant phase according to Refs. [32,33]. Numerical methods, such as density-matrix renormalization group [34] or quantum Monte Carlo simulations [35], are used to study the quantum phase transition in the RLM, while most results are restricted to one-dimensional systems with finite sites which are far away from the thermodynamic limit.

This paper is motivated by the previous paper Ref. [30], while we propose a clearer polaritonic excitation picture to understand this quantum phase transition from insulator to delocalized superradiant phase and introduce the parameter $m = \langle G|\hat{a}^\dagger \hat{a}|G\rangle$ to describe the quantum fluctuation of the TLS on the ground state. The CRC induces a long-range Ising-like interaction among intersite TLSs. Through the Bogoliubov transformation, the transformed Hamiltonian is diagonalized, and coupled TLSs and photons are hybridized to form the polaritonic states. When the photon hopping J is weak, the system is in the insulator phase and the excitation spectrum is gapped. But the gap closes at critical value $J = J_c$ and the ground state becomes instable. Thus, J_c is the phase transition point where the polaritons are condensed at the Γ point to form the delocalized superradiant phase. As the quantum fluctuation is important around the critical point, the introduced parameter m further improves the approximation method used in Ref. [30]. The results show that the phase boundary is dependent on the parameter m, in Sec. II.

In this paper, we demonstrate the polaritonic excitation behaviors and insulator-to-superradiant phase quantum phase transition in much broad parameter space beyond the resonance case $\varepsilon = \omega$ in Ref. [30]. The quantitative research of off-resonant situations illustrates the influence of detuning on the phase transition boundary. Larger detuning indicates a stronger transverse field, which favors the local disorder phase. Thus, the increase of the relative detuning contributes to the stronger fluctuations, and the higher critical hopping coupling J_c to reach the long-range order phase. Additionally, our results show in the strong-coupling case that the RLM reduces to the transverse field Ising model, which indicates that the insulator-to-superradiant phase transition belongs to the Ising university class. Comparing with mean-field theory (MFT) and strong-coupling limit results, we confirm the validity of our method.

This paper is organized as follows. In Sec. II, we introduce the unitary transformations to study the strongly correlated effects in the RLM, while maintaining the CRC terms in the intrasite coupling. In Sec. III, the Bogoliubov transformation is used to diagonalize the transformed Hamiltonian of the RLM. The corresponding ground state and polaritonic excitation spectra in the insulator phase are calculated. The Bose-Einstein condensation of the polaritons triggers insulator-to-superradiant quantum phase transition. The equations to determine the parameters of unitary transformation are solved numerically, in Sec. IV. Then, the phase boundary of the quantum phase transition is obtained, and the results are compared with the mean-field and strong-coupling results. In Sec. V, we introduce another transformation $\hat{R}$ to displace the $\boldsymbol{k} = 0$ mode. The gapped

excitation in the delocalized superradiant phase and the order parameter are explored. Finally, we conclude our paper in Sec. VI.

II. UNITARY TRANSFORMATION METHOD

In order to take into account the effect of CRC terms, we perform the displaced transformation $\hat{S}_1$ and the squeezing transformation $\hat{S}_2$ on $\hat{H}$, where

$$\hat{S}_1 = \frac{1}{\sqrt{N}}\sum_{\boldsymbol{k}}\sum_i \frac{g\xi_{\boldsymbol{k}}}{\omega_{\boldsymbol{k}}}\hat{\sigma}_i^x(\hat{b}_{-\boldsymbol{k}}^\dagger - \hat{b}_{\boldsymbol{k}})e^{-i\boldsymbol{k}\boldsymbol{r}_i}, \tag{4}$$

$$\hat{S}_2 = \frac{1}{2}\sum_{\boldsymbol{k}} \ln(\tau_{\boldsymbol{k}})(\hat{b}_{\boldsymbol{k}}\hat{b}_{-\boldsymbol{k}} - \hat{b}_{\boldsymbol{k}}^\dagger\hat{b}_{-\boldsymbol{k}}^\dagger), \tag{5}$$

where $\hat{b}_{\boldsymbol{k}}$ is the Fourier form of the creation (annihilation) operator with frequency $\omega_{\boldsymbol{k}} = \omega - zJ\gamma(\boldsymbol{k})$ (z the coordinate number), and the lattice dispersion $\gamma(\boldsymbol{k}) = [\cos(k_x) + \cos(k_y)]/2$ for the two-dimensional square lattice. The displacement parameters $\xi_{\boldsymbol{k}}$ and the squeezing parameters $\tau_{\boldsymbol{k}}$ are determined in the latter to eliminate the CRC terms in $\hat{H}$.

The unitary transformation on Hamiltonian $\hat{H}' = e^{\hat{S}_2}e^{\hat{S}_1}\hat{H}e^{-\hat{S}_1}e^{-\hat{S}_2}$ can be done straightforwardly to the end without introducing any approximation. The transformed Hamiltonian is constructed in the form $\hat{H}' = \hat{H}_0' + \hat{H}_1' + \hat{H}_2'$, where

$$\begin{aligned}\hat{H}_0' = {}& \frac{N\epsilon}{2} - NV_0 + \sum_i \frac{\eta\epsilon\hat{\sigma}_i^z}{2} \\ & + \sum_{\boldsymbol{k}} \frac{\omega_{\boldsymbol{k}}}{4}\left[\tau_{\boldsymbol{k}}^2|\hat{b}_{-\boldsymbol{k}}^\dagger + \hat{b}_{\boldsymbol{k}}|^2 - \tau_{\boldsymbol{k}}^{-2}|\hat{b}_{-\boldsymbol{k}}^\dagger - \hat{b}_{\boldsymbol{k}}|^2 - 2\right] \\ & + \frac{1}{N}\sum_i\sum_{\boldsymbol{k}} \frac{\eta\epsilon g^2\xi_{\boldsymbol{k}}^2}{\omega_{\boldsymbol{k}}^2\tau_{\boldsymbol{k}}^2}\hat{\sigma}_i^z(\hat{b}_{\boldsymbol{k}}^\dagger\hat{b}_{-\boldsymbol{k}}^\dagger + \hat{b}_{\boldsymbol{k}}\hat{b}_{-\boldsymbol{k}} - 2\hat{b}_{\boldsymbol{k}}^\dagger\hat{b}_{\boldsymbol{k}}) \\ & - \frac{1}{N}\sum_{i,j}\hat{\sigma}_i^x\hat{\sigma}_j^x\sum_{\boldsymbol{k}}\left[\frac{g^2}{\omega_{\boldsymbol{k}}}\xi_{\boldsymbol{k}}(2-\xi_{\boldsymbol{k}}) - V_0\right]e^{i\boldsymbol{k}(\boldsymbol{r}_i-\boldsymbol{r}_j)}, \end{aligned} \tag{6}$$

$$\begin{aligned}\hat{H}_1' = {}& \frac{1}{\sqrt{N}}\sum_{\boldsymbol{k}}\sum_i g(1-\xi_{\boldsymbol{k}})\tau_{\boldsymbol{k}}\hat{\sigma}_i^x(\hat{b}_{-\boldsymbol{k}}^\dagger + \hat{b}_{\boldsymbol{k}})e^{-i\boldsymbol{k}\boldsymbol{r}_i} \\ & - \frac{1}{\sqrt{N}}\sum_{\boldsymbol{k}}\sum_i \frac{\eta\epsilon g\xi_{\boldsymbol{k}}}{\omega_{\boldsymbol{k}}\tau_{\boldsymbol{k}}}i\hat{\sigma}_i^y(\hat{b}_{-\boldsymbol{k}}^\dagger - \hat{b}_{\boldsymbol{k}})e^{-i\boldsymbol{k}\boldsymbol{r}_i}, \end{aligned} \tag{7}$$

$$\begin{aligned}\hat{H}_2' = {}& -\frac{\epsilon}{2}\sum_i i\hat{\sigma}_i^y[\sinh(\hat{X}_i) - \eta\hat{X}_i] + \frac{\epsilon}{2}\sum_i\hat{\sigma}_i^z\Bigg[\cosh(\hat{X}_i) \\ & - \eta - \frac{1}{N}\sum_{\boldsymbol{k}}\frac{\eta\epsilon g^2\xi_{\boldsymbol{k}}^2}{\omega_{\boldsymbol{k}}^2\tau_{\boldsymbol{k}}^2}(\hat{b}_{\boldsymbol{k}}^\dagger\hat{b}_{-\boldsymbol{k}}^\dagger + \hat{b}_{\boldsymbol{k}}\hat{b}_{-\boldsymbol{k}} - 2\hat{b}_{\boldsymbol{k}}^\dagger\hat{b}_{\boldsymbol{k}})\Bigg], \end{aligned} \tag{8}$$

where the operator $\hat{X}_i$ is introduced as

$$\hat{X}_i \equiv \frac{2}{\sqrt{N}}\sum_{\boldsymbol{k}}\frac{g\xi_{\boldsymbol{k}}}{\omega_{\boldsymbol{k}}\tau_{\boldsymbol{k}}}(\hat{b}_{-\boldsymbol{k}}^\dagger - \hat{b}_{\boldsymbol{k}})e^{-i\boldsymbol{k}\boldsymbol{r}_i}, \tag{9}$$

and the parameters η and V_0 are defined as

$$\eta \equiv \exp\left(-\frac{2}{N}\sum_{\boldsymbol{k}}\frac{g^2\xi_{\boldsymbol{k}}^2}{\omega_{\boldsymbol{k}}^2\tau_{\boldsymbol{k}}^2}\right), \tag{10}$$

$$V_0 \equiv \frac{1}{N}\sum_{\boldsymbol{k}}\frac{g^2\xi_{\boldsymbol{k}}}{\omega_{\boldsymbol{k}}}(2-\xi_{\boldsymbol{k}}). \tag{11}$$

The last term in $\hat{H}_0'$ describes the long-range Ising-like interaction among the intersite TLSs, and V_0 is subtracted to eliminate a constant self-interaction at the same site.

The dominant parts that remain in the $\hat{H}_2'$ are the products of three or more photon operators in normal ordering. As we focus on the ground and low-lying excited states, the effect of multiphoton processes is weak, which makes it reasonable to drop $\hat{H}_2'$ in the following calculation. It is worth emphasizing that the neglect of $\hat{H}_2'$ does not mean that our result is valid only to the second order of g. The photon-dressing parameter η, introduced in Eq. (10), includes the infinite order of g, which is involved in the form of $\hat{H}_0'$ and $\hat{H}_1'$. Thus, with the parameter η, the strong-coupling effects on the ground and low-lying excited states can be explored to a satisfactory degree. We think that our results work well even for the strong-coupling case. In fact, as we show in Sec. IV B, in the strong-coupling case, the RLM reduces to the quantum transverse Ising model. The accuracy of this method has been confirmed by the single- and double-site Rabi model at the resonant condition $\epsilon = \omega$ in Ref. [30].

III. INSULATING PHASE

We use the Holstein-Primakoff (HP) transformation to turn the Pauli matrices in $\hat{H}' \simeq \hat{H}_0' + \hat{H}_1'$ into the bosonic operators $\hat{a}_i$ and $\hat{a}_i^\dagger$ [36],

$$\hat{\sigma}_i^x = \hat{a}_i^\dagger\sqrt{1-\hat{a}_i^\dagger\hat{a}_i} + \sqrt{1-\hat{a}_i^\dagger\hat{a}_i}\hat{a}_i, \tag{12}$$

$$i\hat{\sigma}_i^y = \hat{a}_i^\dagger\sqrt{1-\hat{a}_i^\dagger\hat{a}_i} - \sqrt{1-\hat{a}_i^\dagger\hat{a}_i}\hat{a}_i, \tag{13}$$

$$\hat{\sigma}_i^z = 2\hat{a}_i^\dagger\hat{a}_i - 1, \tag{14}$$

and then apply the mean-field approximation:

$$\hat{\sigma}_i^x \simeq \sqrt{1-m}(\hat{a}_i^\dagger + \hat{a}_i), \tag{15}$$

$$i\hat{\sigma}_i^y \simeq \sqrt{1-m}(\hat{a}_i^\dagger - \hat{a}_i). \tag{16}$$

The parameter m is the mean value of $\hat{a}_i^\dagger\hat{a}_i$ on the ground state of $\hat{H}'$, $m \equiv \langle G'|\hat{a}_i^\dagger\hat{a}_i|G'\rangle$, and will be determined in the self-consistent way. Compared with linearized spin-wave approximation [30], the HP transformation involves the quantum fluctuation of the TLS on the ground state.

Then, $\hat{H}' \simeq H^I$ is approximated as

$$\begin{aligned}H^I = {}& \frac{1-\eta}{2}N\epsilon - NV_0 + \sum_{\boldsymbol{k}}\frac{\omega_{\boldsymbol{k}}}{4}\left(\tau_{\boldsymbol{k}}^2 + \tau_{\boldsymbol{k}}^{-2} - 2\right) \\ & + \sum_{\boldsymbol{k}}\omega_{\boldsymbol{k}}\tau_{\boldsymbol{k}}^2\hat{b}_{\boldsymbol{k}}^\dagger\hat{b}_{\boldsymbol{k}} + \sum_{\boldsymbol{k}}\eta\epsilon\hat{a}_{\boldsymbol{k}}^\dagger\hat{a}_{\boldsymbol{k}} \\ & - (1-m)\sum_{\boldsymbol{k}}\left[\frac{g^2}{\omega_{\boldsymbol{k}}}\xi_{\boldsymbol{k}}(2-\xi_{\boldsymbol{k}}) - V_0\right](\hat{a}_{-\boldsymbol{k}}^\dagger + \hat{a}_{\boldsymbol{k}})(\hat{a}_{\boldsymbol{k}}^\dagger + \hat{a}_{-\boldsymbol{k}}) \\ & + \sqrt{(1-m)}\sum_{\boldsymbol{k}} g(1-\xi_{\boldsymbol{k}})\tau_{\boldsymbol{k}}(\hat{b}_{-\boldsymbol{k}}^\dagger + \hat{b}_{\boldsymbol{k}})(\hat{a}_{\boldsymbol{k}}^\dagger + \hat{a}_{-\boldsymbol{k}}) \\ & - \sqrt{(1-m)}\sum_{\boldsymbol{k}}\frac{\eta\epsilon g\xi_{\boldsymbol{k}}}{\omega_{\boldsymbol{k}}\tau_{\boldsymbol{k}}}(\hat{b}_{-\boldsymbol{k}}^\dagger - \hat{b}_{\boldsymbol{k}})(\hat{a}_{\boldsymbol{k}}^\dagger - \hat{a}_{-\boldsymbol{k}}) \end{aligned} \tag{17}$$

with

$$\tau_k^2 = \sqrt{1 + 4\eta\epsilon g^2 \xi_k^2/\omega_k^3}. \tag{18}$$

The Hamiltonian H^I can be diagonalized by another Bogoliubov transformation $\hat{S}_3$, where $\hat{S}_3 = \frac{1}{2}\sum_k \ln(\rho_k^{-1})(\hat{a}_k\hat{a}_{-k} - \hat{a}_k^\dagger\hat{a}_{-k}^\dagger)$, with ξ_k and ρ_k given by

$$\xi_k = \frac{\omega_k\tau_k^2}{\omega_k\tau_k^2 + \eta\epsilon\rho_k^2}, \tag{19}$$

$$\rho_k^2 = \sqrt{1 - \frac{4(1-m)}{\eta\epsilon}\left[\frac{g^2\xi_k(2-\xi_k)}{\omega_k} - V_0\right]}. \tag{20}$$

After the Bogoliubov transformation, the Hamiltonian becomes

$$e^{\hat{S}_3}\hat{H}^I e^{-\hat{S}_3} = E_g^I + \sum_k \omega_k\tau_k^2\hat{b}_k^\dagger\hat{b}_k + \sum_k \eta\epsilon\rho_k^2\hat{a}_k^\dagger\hat{a}_k + \sum_k g_{Ik}(\hat{b}_k^\dagger\hat{a}_k + \hat{b}_k\hat{a}_k^\dagger), \tag{21}$$

where $g_{Ik} = 2\sqrt{(1-m)}g\tau_k(1-\xi_k)\rho_k^{-1}$ is the effective coupling strength between the TLS and the photon. With the choice of parameters ξ_k, τ_k, and ρ_k, the transformed Hamiltonian $e^{\hat{S}_3}\hat{H}^I e^{-\hat{S}_3}$ takes on a RWA-like form. Through the renormalized quantities g_{Ik}, $\epsilon\eta\rho_k^2$, and $\omega_k\tau_k$, the effects of the CRC terms are explored. Then, it is easy to get the diagonalized Hamiltonian in the polariton picture:

$$\hat{H} = E_g^I + \textstyle\sum_k E_I^\pm(\boldsymbol{k})\hat{d}_{\pm k}^\dagger\hat{d}_{\pm k},$$

where

$$\hat{d}_{-k} = \cos\alpha\hat{a}_k - \sin\alpha\hat{b}_k, \tag{22}$$

$$\hat{d}_{+k} = \sin\alpha\hat{a}_k + \cos\alpha\hat{b}_k, \tag{23}$$

with $\tan 2\alpha = 2g_{Ik}/(\omega_k\tau_k^2 - \eta\epsilon\rho_k^2)$. The ground state of $\hat{H}^I$ is in the form of $|G_I\rangle = |\{\hat{d}_{\pm k}^\dagger\hat{d}_{\pm k} = 0\}\rangle$ and the corresponding ground-state energy of the insulating phase is

$$E_g^I = \frac{1-2\eta}{2}N\epsilon - NV_0 + \sum_k \frac{\omega_k}{4}\left(\tau_k^2 + \tau_k^{-2} - 2\right) + \sum_k \frac{\eta\epsilon}{2}\rho_k^2. \tag{24}$$

From the ground state $|G_I\rangle$, we can get the self-consistent equation of m as

$$m = \langle G_I|e^{\hat{S}_3}\hat{a}_i^\dagger\hat{a}_i e^{-\hat{S}_3}|G_I\rangle = \frac{1}{4N}\sum_k\left(\rho_k^{-2} + \rho_k^2 - 2\right). \tag{25}$$

In the insulating phase, the excitation energies of polaritons have two branches $E_I^\pm(\boldsymbol{k})$, and the analytic formulas for the dispersion relations are

$$E_I^\pm(\boldsymbol{k}) = \frac{1}{2}\left(\eta\epsilon\rho_k^2 + \omega_k\tau_k^2\right) \pm \frac{1}{2}\sqrt{\left(\eta\epsilon\rho_k^2 - \omega_k\tau_k^2\right)^2 + 4g_{Ik}^2}. \tag{26}$$

In the weak-coupling limit, $\omega, J \gg g$, as a crude approximation, the TLS and photon almost decouple. The TLS stays on its respective ground state, and the system has a flat band with the energy splitting ϵ contribution from the atomic excitation. The photonic excitation contributes from the bosonic tight-binding model with the dispersion relation ω_k. Through the Bogoliubov transformation, our results show that the polariton emerges from the hybridized system where TLSs and the photons are coupled with the effective coupling strength g_{Ik}. The dispersion relation of the two-branch polaritonic excitations $E_I^\pm(\boldsymbol{k})$ for the two-dimensional square lattice is plotted in Fig. 2(a) for the negative detuning case $\Delta = -0.1\omega$, Fig. 2(b) for the resonant case $\Delta = 0$, and Fig. 2(c) for the positive detuning case $\Delta = 0.1\omega$ deep inside the insulator phase with $\omega = 1.5g$. The important features in Figs. 2(a)–2(c) are that the polaritonic excitation spectra in the insulator state are characterized by gapped cosinelike bands, and have their minima at $\boldsymbol{k} = \boldsymbol{0}$.

The branch $E_I^-(\boldsymbol{k})$ always has the lower excitation energy, and the dispersion relations of $E_I^-(\boldsymbol{k})$ around the critical point for the two-dimensional square lattice are plotted in Figs. 2(d)–2(f). In the negative detuning case $\Delta = -0.1\omega$, the results show that there exists a gap at $\boldsymbol{k} = 0$ in the insulator phase $zJ/g = 0.280$. The gap $E_I^-(\boldsymbol{0})$ decreases with increasing of the hopping strength J, and eventually closes at the critical point, $zJ_c/g = 0.321\,67$, with linear dispersion at small $\boldsymbol{k}$ in Fig. 2(d). Similar behaviors are also found for the resonant case $\Delta = 0$, where the gap $E_I^-(\boldsymbol{0})$ closes at the critical point $zJ_c/g = 0.352\,93$ but opens at $zJ/g = 0.320$ in Fig. 2(e). For the positive detuning case $\Delta = 0.1\omega$ in Fig. 2(f), there exists a gap at $zJ/g = 0.350$ in the insulator phase while the gap $E_I^-(\boldsymbol{0})$ disappears at the critical point $zJ_c/g = 0.383\,18$. The results confirm that below the critical hoping strength J_c the systems have a stable insulating ground state. Above J_c, $E_I^-(\boldsymbol{0})$ becomes negative. In this case, adding more polaritons to the system always lowers the total energy, which means the system becomes unstable. Then, macroscopic polaritons occupy the ground state, and the Bose-Einstein condensation of the polaritons emerges.

The condensation of the polariton gives rise to instability of the insulator phase, and triggers the phase transition to the delocalized superradiant phase. Therefore, the condition for the presence of the stable insulating phase can be used as a criterion to determine the boundary of the phase transition:

$$\eta\epsilon\rho_{\boldsymbol{0}}^2\omega_{\boldsymbol{0}}\tau_{\boldsymbol{0}}^2 \geqslant g_{I\boldsymbol{0}}^2 \quad \Rightarrow \quad 2(1-m)G_{\boldsymbol{0}} \leqslant \eta\epsilon, \tag{27}$$

where $G_{\boldsymbol{0}} = 2g^2/\omega_{\boldsymbol{0}} - 2V_0$. As the coupled TLSs and photons are hybridized to form the polaritonic states, the fluctuations of the TLS should be taken into account to give the effects on the phase boundary, which are described by the parameter m in Eq. (27).

The boundary of the phase transition is determined by

$$2(1-m_c)G_{\boldsymbol{0}} = \eta\epsilon, \tag{28}$$

where m at the phase transition point is noted as m_c. The phase boundary is dependent on the parameter m. The stronger the fluctuation on the TLS, the higher the critical hopping coupling J_c required to reach the long-range order phase. In Fig. 2, $m_c = 0.027\,54$ in the negative detuning case with $\Delta = -0.1\omega$ and $zJ/g = 0.250$, $m_c = 0.024\,49$ in the resonant case with $\Delta = 0$ and $zJ/g = 0.225$, and $m_c = 0.021\,76$ in the

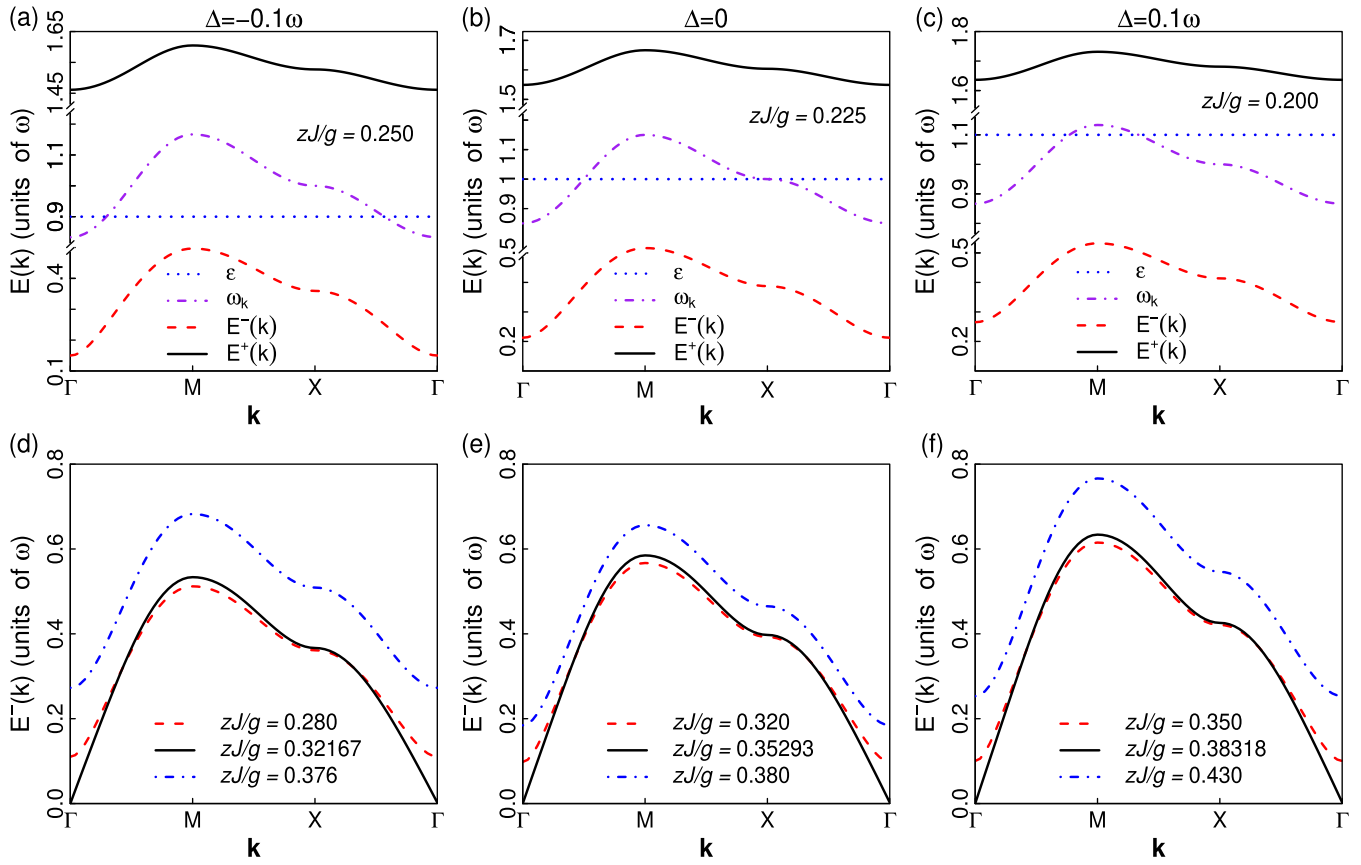

FIG. 2. (a–c) The dispersion relation of the two-branch polaritonic excitations $E_l^{\pm}(\boldsymbol{k})$ for the two-dimensional square lattice RLM at $\omega = 1.5g$: (a) the negative detuning case with $\Delta = -0.1\omega$ and $zJ/g = 0.250$; (b) the resonant case with $\Delta = 0$ and $zJ/g = 0.225$; (c) the positive detuning case with $\Delta = 0.1\omega$ and $zJ/g = 0.200$. (d–f) The dispersion relation of the low-branch polaritonic excitations $E^{-}(\boldsymbol{k})$ for the two-dimensional square lattice RLM at $\omega = 1.5g$ around the critical points: (d) the negative relative detuning case with $\Delta = -0.1\omega$ and $zJ/g = 0.250$; (e) the resonant case with $\Delta = 0$ and $zJ/g = 0.225$; (f) the positive relative detuning case with $\Delta = 0.1\omega$ and $zJ/g = 0.200$. Energies are in the units of ω.

positive detuning case with $\Delta = 0.1\omega$ and $zJ/g = 0.200$ in the two-dimensional square lattice RLM. In order to show precisely the effect of quantum fluctuations, the values of the parameter m_c at the critical points as a function of detuning Δ with several different photon frequencies ω are shown in Fig. 3.

IV. PHASE DIAGRAM

The phase diagram is an important feature to characterize the phase transition. In this section, we show the phase diagram of the insulator-to-superradiant quantum phase transition on the two-dimensional square lattice RLM.

A. Mean-field theory

The main idea in MFT is that it neglects the fluctuations between the operators. In the scheme of MFT, the hopping terms in the RLM are decoupled as

$$\hat{b}_i^{\dagger}\hat{b}_j = \langle \hat{b}_i^{\dagger}\rangle \hat{b}_j + \hat{b}_i^{\dagger}\langle \hat{b}_j\rangle - \langle \hat{b}_i^{\dagger}\rangle\langle \hat{b}_j\rangle, \tag{29}$$

and $\langle \hat{b}_j\rangle$ is replaced by the order parameter ψ. Then, the original RLM reduces to a single site problem with the effective

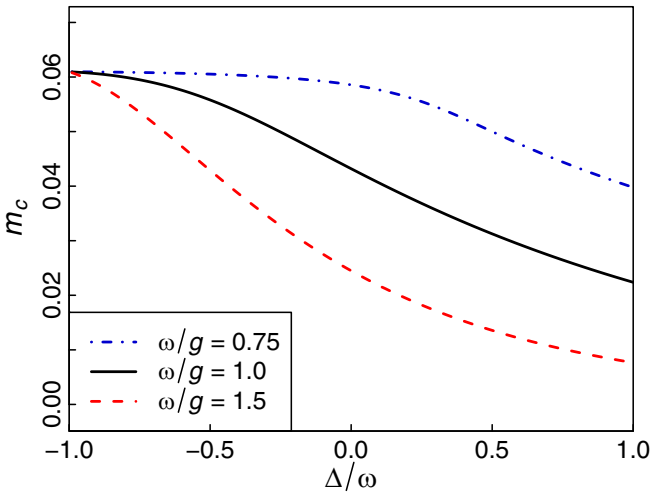

FIG. 3. The value of the dimensionless parameter m_c at the critical points as a function of detuning Δ with several different photon frequencies ω.

Hamiltonian

$$\hat{H} \simeq \sum_i \left[\hat{H}_i^R - zJ\psi(\hat{b}_i^\dagger + \hat{b}_i) + zJ\psi^2\right]. \tag{30}$$

Around the critical point, the order parameter ψ is small. ψ can be calculated in the perturbation theory [27,32]. As a result, the expression of the perturbation ground energy in the power of ψ is

$$\frac{E_g^{\mathrm{MF}}}{N} = E_0 + zJ\psi^2 + (zJ)^2 \sum_{n\neq 0} \frac{\langle n|(\hat{b}^\dagger + \hat{b})|0\rangle^2}{E_0 - E_n}\psi^2, \tag{31}$$

where $|n\rangle$ represents the exact nth eigenstate of the single site Rabi model, and E_n is the corresponding eigenenergy. The analytic solution of the Rabi model was found [37–39]. In the spirit of Landau theory the second-order terms being zero indicates a phase transition. Then, the full phase transition boundary is obtained as

$$\frac{1}{zJ_c} = \sum_{n\neq 0} \frac{\langle n|(\hat{b}^\dagger + \hat{b})|0\rangle^2}{E_n - E_0}. \tag{32}$$

Similarly, one can also get the insulator-to-superfluid phase transition boundary of the JCLM [27].

Above the phase transition point, the parameter ψ is not small, and the Gutzwiller solution [16] can be used to self-consistently determine ψ. At first, ψ is set with a random initial value, and the Hamiltonian is numerically diagonalized to give a better estimation of ψ. This process will iteratively continue until the ground state converges. Then, we can obtain the order parameter ψ as a function of zJ in MFT.

B. Strong-coupling limit, $g \gg \omega$

In the strong-coupling limit $g \gg \omega$, from Eqs. (18) and (19), we have $\tau_{\boldsymbol{k}} = 1$ and $\xi_{\boldsymbol{k}} = 1$. For the weak hopping coupling, $\omega \gg J$, the ground state corresponds to the photon vacuum state. The averaging of the Hamiltonian $\hat{H}_0 + \hat{H}_1'$ over the photon vacuum produces the quantum transverse field Ising model (QTFI) [31,34]:

$$\hat{H}_{\mathrm{QI}} = \frac{N\epsilon}{2} + \frac{Ng^2}{\omega} + \frac{\eta\epsilon}{2}\sum_i \hat{\sigma}_i^z - 2J\frac{g^2}{\omega^2}\sum_{\langle i,j\rangle} \hat{\sigma}_i^x \hat{\sigma}_j^x, \tag{33}$$

where the effective transverse field is $h = \eta\epsilon/2$, and the Ising interaction $t = 2Jg^2/\omega^2$. The QTFI is a well-studied physical model, and the system undergoes a quantum phase transition from a paramagnetic phase to a ferromagnetic phase. The exact quantum critical point for the one-dimensional spin chain is $t/h = 1$ [40,41], and the numerical result for the two-dimensional square lattice is $t/h \simeq 0.328$ [42,43]. Therefore, the strong-coupling critical hopping is $J_c = \frac{\epsilon\omega^2}{4g^2}\exp(-2g^2/\omega)$ for the one-dimensional spin chain, and $J_c = \frac{0.328\epsilon\omega^2}{4g^2}\exp(-2g^2/\omega)$ for the two-dimensional square lattice.

These strong-coupling results support the gapped excitation in the delocalized superradiant phase and indicate that the insulator-to-superradiant phase transition belongs to the Ising university class, which is confirmed by quantum Monte Carlo simulations [35].

C. Numerical results

The phase boundary is determined by Eq. (28), and the equations to determine the parameters can be solved numerically. Taking the parameters in the insulator phase as an example, we briefly explain how to get the numerical solutions of the parameter equations. There are two types of parameters: the $\boldsymbol{k}$-dependent parameters, i.e., $\xi_{\boldsymbol{k}}$, $\tau_{\boldsymbol{k}}$, and $\rho_{\boldsymbol{k}}$, and the $\boldsymbol{k}$-independent parameters, i.e., V_0, η, and m, which are defined by the integral of the function of the $\boldsymbol{k}$-dependent parameters in Eqs. (10), (11), and (25). At first, V_0, η, and m are set with random initial values, and then we can calculate $\xi_{\boldsymbol{k}}$, $\tau_{\boldsymbol{k}}$, and $\rho_{\boldsymbol{k}}$ by Eqs. (18)–(20). Using Eqs. (10), (11), and (25), we can get a better estimation of V_0, η, and m. This process will iteratively continue until the values of the parameter converge. During the process, for each fixed V_0, η, and m, the $\boldsymbol{k}$-dependent parameters $\xi_{\boldsymbol{k}}$, $\tau_{\boldsymbol{k}}$, and $\rho_{\boldsymbol{k}}$ also need another similar iterative process to get the numerical values. As a result, we can get the numerical solutions of the parameter equations.

In this subsection, we show the numerical results of the phase boundary, and illustrate the validity of the different approximation methods. The phase diagrams in the $(zJ/g, \omega/g)$ plane for the negative detuning case $\Delta = -0.1\omega$, the resonant condition $\omega = \epsilon$, and the positive detuning case $\Delta = 0.1\omega$

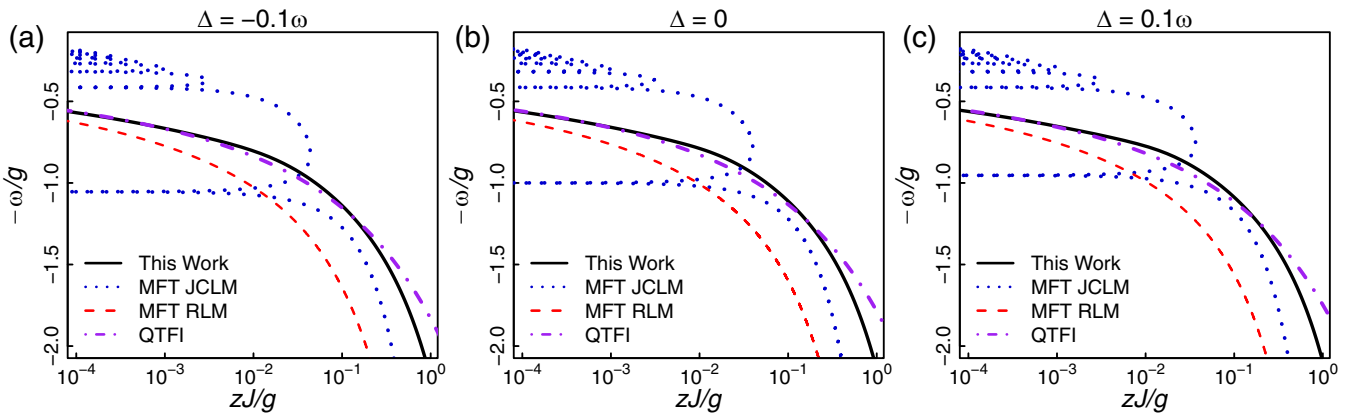

FIG. 4. The phase diagram of the two-dimensional RLM obtained by the different approximation methods, in the $(zJ/g, \omega/g)$ plane with a logarithmic horizontal axis: (a) the negative detuning case $\Delta = -0.1\omega$; (b) the resonant case $\Delta = 0$; (c) the positive detuning case $\Delta = 0.1\omega$.

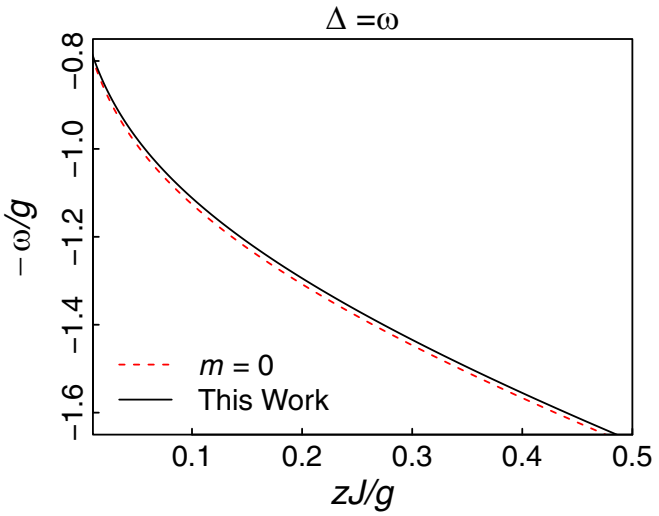

FIG. 5. The phase boundary of the two-dimensional RLM at the resonant condition $\omega = \epsilon$. The introduced parameter m involves visible influences on the phase boundary.

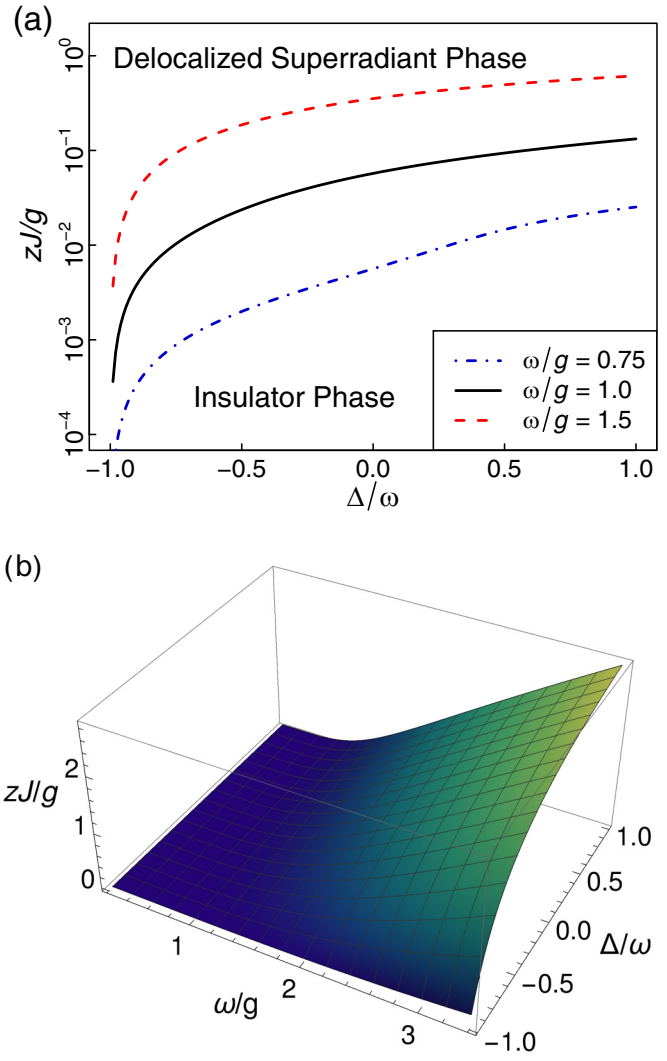

FIG. 6. The phase boundary of the two-dimensional RLM (a) in the $(zJ/g, \Delta/\omega)$ plane with fixed $\omega/g = 0.75, 1, 1.5$ with a logarithmic vertical axis and (b) in the general $(\omega/g, \Delta/\omega, zJ/g)$ space.

are shown with the solid line in Fig. 4. For comparison, the phase diagrams obtained by MFT and QTFI are also shown. For the MFT on JCLM, the phase boundary has the analog lobes of the Mott-insulator phase in the Bose-Hubbard model. However, as the polariton number conservation is broken in the RLM, both the MFT and our results show the absence of the lobes. The MFT on the RLM gives the qualitatively correct phase diagram, while it neglects the fluctuation of the photons which can destroy the long-range order. As a result, the critical hopping zJ_c in the MFT is always smaller than our results. In the strong-coupling situation $g \gg \omega$, the QTFI shows the critical hopping $J_c = \frac{0.328\epsilon}{4}\frac{\omega^2}{g^2}\exp(-2g^2/\omega)$. Our results are consistent with the QTFI in the strong-coupling case $g \gg \omega$, while the deviation of the two methods is emerging in the case $g < \omega$.

Comparing the phase diagram in plane $(zJ/g, \omega/g)$ obtained by different approximation methods, we show that the fluctuations of the photon are important around the critical point. In this paper, we also involve the fluctuations of the TLS by the introduced parameter m. As an example, the phase diagram of the two-dimensional RLM at the resonant condition $\omega = \epsilon$ is plotted in Fig. 5. Compared with the previous results in Ref. [30] where the m are neglected, there exist visible differences between the results from the two approaches. According to the phase boundary, i.e., $2(1-m)G_0 = \eta\epsilon$, stronger the fluctuation on the TLS, the higher the critical hopping coupling J_c required to reach the long-range order phase.

To get a better description of the phase transition, we further illustrate the influences of the detuning on the phase transition boundary in Fig. 6(a). The detuning, $\Delta = \epsilon - \omega$, between the two-level energy splitting and the cavity photon frequency is another important parameter in the RLM, which is easily manipulated in experiments [44]. In Fig. 6(a), we plot the phase boundary in the $(zJ/g, \Delta/\omega)$ plane for the different fixed values of ω. The insulating phase is stable until the critical hopping coupling J_c, above which the long-range order superradiant phase emerges. By Eq. (6), one knows that a larger detuning indicates a stronger transverse field $\frac{\epsilon\eta}{2}\hat{\sigma}_z$, which favors the local disorder phase. Thus, the increase of the relative detuning contributes to the stronger fluctuation, and the higher critical hopping coupling J_c to reach the long-range order phase, which is confirmed in Fig. 6(a).

Finally, in Fig. 6(b), we overview the phase diagram for the two-dimensional RLM with the general detuning in the $(\omega/g, \Delta/\omega, zJ/g)$ space. Above the surface, the insulator phase is no longer stable and the delocalized superradiant phase emerges.

V. DELOCALIZED SUPERRADIANT PHASE

For the case $2(1-m)G_0 > \eta\epsilon$, macroscopic polaritons condense in the ground state, and the system is in the delocalized superradiant phase. In this phase, the order parameter $\langle G|\hat{b}|G\rangle \neq 0$, so another static displacement of the $\boldsymbol{k} = 0$

photon mode is required. Here, we perform the unity transformation $\hat{R}$ on $\hat{H}_0'$ and $\hat{H}_1'$ as

$$\begin{aligned} e^{\hat{R}}(\hat{H}_0'+\hat{H}_1')e^{-\hat{R}} =& \frac{N\epsilon}{2} - NV_0 + \frac{N(1-m_c)^2G_0\sigma_0^2}{2} + \sum_i (1-m_c)G_0\sigma_0\hat{\sigma}_i^x + \sum_i \frac{\eta\epsilon\hat{\sigma}_i^z}{2} \\ &+ \sum_{\boldsymbol{k}} \frac{\omega_{\boldsymbol{k}}}{4}\left[\tau_{\boldsymbol{k}}^2|\hat{b}_{-\boldsymbol{k}}^\dagger + \hat{b}_{\boldsymbol{k}}|^2 - \tau_{\boldsymbol{k}}^{-2}|\hat{b}_{-\boldsymbol{k}}^\dagger - \hat{b}_{\boldsymbol{k}}|^2 - 2\right] + \frac{1}{N}\sum_i\sum_{\boldsymbol{k}} \frac{\eta\epsilon g^2\xi_{\boldsymbol{k}}^2}{\omega_{\boldsymbol{k}}^2\tau_{\boldsymbol{k}}^2}(\hat{b}_{\boldsymbol{k}}^\dagger\hat{b}_{-\boldsymbol{k}}^\dagger + \hat{b}_{\boldsymbol{k}}\hat{b}_{-\boldsymbol{k}} - 2\hat{b}_{\boldsymbol{k}}^\dagger\hat{b}_{\boldsymbol{k}})\hat{\sigma}_i^z \\ &- \frac{1}{N}\sum_{i,j}\left[\hat{\sigma}_i^x + (1-m_c)\sigma_0\right]\left[\hat{\sigma}_j^x + (1-m_c)\sigma_0\right] \times \sum_{\boldsymbol{k}}\left[\frac{g^2}{\omega_{\boldsymbol{k}}}\xi_{\boldsymbol{k}}(2-\xi_{\boldsymbol{k}}) - V_0\right]e^{i\boldsymbol{k}(\boldsymbol{r}_i-\boldsymbol{r}_j)} \\ &+ \frac{1}{\sqrt{N}}\sum_{\boldsymbol{k}}\sum_i g(1-\xi_{\boldsymbol{k}})\tau_{\boldsymbol{k}}\left[\hat{\sigma}_i^x + (1-m_c)\sigma_0\right](\hat{b}_{-\boldsymbol{k}}^\dagger + \hat{b}_{\boldsymbol{k}})e^{-i\boldsymbol{k}\boldsymbol{r}_i} - \frac{1}{\sqrt{N}}\sum_{\boldsymbol{k}}\sum_i \frac{\eta\epsilon g\xi_{\boldsymbol{k}}}{\omega_{\boldsymbol{k}}\tau_{\boldsymbol{k}}} i\hat{\sigma}_i^y(\hat{b}_{-\boldsymbol{k}}^\dagger - \hat{b}_{\boldsymbol{k}})e^{-i\boldsymbol{k}\boldsymbol{r}_i}, \end{aligned} \tag{34}$$

where the generator of the transformation is given by

$$\hat{R} = -(1-m_c)\frac{\sqrt{N}g(1-\xi_{\boldsymbol{0}})}{\omega_{\boldsymbol{0}}\tau_{\boldsymbol{0}}}\sigma_0(\hat{b}_{\boldsymbol{0}}^\dagger - \hat{b}_{\boldsymbol{0}}). \tag{35}$$

Before we apply HP transformation, we rotate the Pauli matrices at every site i with a unitary matrix U_i to get

$$U_i^\dagger\left[\frac{\eta\epsilon\hat{\sigma}_i^z}{2} + (1-m_c)G_0\sigma_0\hat{\sigma}_i^x\right]U_i = \frac{W}{2}\hat{\sigma}_i^z, \tag{36}$$

with $W = \sqrt{4(1-m_c)^2G_0^2\sigma_0^2 + \epsilon^2\eta^2}$ and $\sigma_0^2 = 1 - \frac{\eta^2\epsilon^2}{4(1-m_c)^2G_0^2}$. For the whole lattice, we have unitary matrix U given by

$$\hat{U} = \prod_i \hat{U}_i. \tag{37}$$

After the rotation, we obtain the expression for $\hat{H}'' = \hat{U}^\dagger e^{\hat{R}}(\hat{H}_0' + \hat{H}_1')e^{-\hat{R}}\hat{U}$ as

$$\begin{aligned} \hat{H}'' =& \frac{N\epsilon}{2} - NV_0 + \frac{N(1-m_c)^2G_0\sigma_0^2}{2} + \sum_{\boldsymbol{k}}\frac{\omega_{\boldsymbol{k}}}{4}\left[\tau_{\boldsymbol{k}}^2|\hat{b}_{-\boldsymbol{k}}^\dagger + \hat{b}_{\boldsymbol{k}}|^2 - \tau_{\boldsymbol{k}}^{-2}|\hat{b}_{-\boldsymbol{k}}^\dagger - \hat{b}_{\boldsymbol{k}}|^2 - 2\right] + \sum_i \frac{W\hat{\sigma}_i^z}{2} \\ &+ \frac{1}{N}\sum_i\sum_{\boldsymbol{k}}\frac{\eta\epsilon g^2\xi_{\boldsymbol{k}}^2}{\omega_{\boldsymbol{k}}^2\tau_{\boldsymbol{k}}^2}(\hat{b}_{\boldsymbol{k}}^\dagger\hat{b}_{-\boldsymbol{k}}^\dagger + \hat{b}_{\boldsymbol{k}}\hat{b}_{-\boldsymbol{k}} - 2\hat{b}_{\boldsymbol{k}}^\dagger\hat{b}_{\boldsymbol{k}})\left(\sigma_0\hat{\sigma}_i^x + \frac{\eta\epsilon}{W}\hat{\sigma}_i^z\right) + \frac{1}{\sqrt{N}}\sum_{\boldsymbol{k}}\sum_i\frac{\eta\epsilon g\xi_{\boldsymbol{k}}}{\omega_{\boldsymbol{k}}\tau_{\boldsymbol{k}}}i\hat{\sigma}_i^y(\hat{b}_{-\boldsymbol{k}}^\dagger - \hat{b}_{\boldsymbol{k}})e^{-i\boldsymbol{k}\boldsymbol{r}_i} \\ &+ \frac{1}{\sqrt{N}}\sum\sum_i g(1-\xi_{\boldsymbol{k}})\tau_{\boldsymbol{k}}\left[-\frac{\eta\epsilon}{W}\hat{\sigma}_i^x + \sigma_0\left(\hat{\sigma}_i^z + 1 - m_c\right)\right](\hat{b}_{-\boldsymbol{k}}^\dagger + \hat{b}_{\boldsymbol{k}})e^{-i\boldsymbol{k}\boldsymbol{r}_i} \\ &- \frac{1}{N}\sum_{i,j,\boldsymbol{k}}\left[-\frac{\eta\epsilon}{W}\hat{\sigma}_i^x + \sigma_0\left(\hat{\sigma}_i^z + 1 - m_c\right)\right]\left[-\frac{\eta\epsilon}{W}\hat{\sigma}_j^x + \sigma_0\left(\hat{\sigma}_j^z + 1 - m_c\right)\right]\left[\frac{g^2}{\omega_{\boldsymbol{k}}}\xi_{\boldsymbol{k}}(2-\xi_{\boldsymbol{k}}) - V_0\right]e^{i\boldsymbol{k}(\boldsymbol{r}_i-\boldsymbol{r}_j)}. \end{aligned} \tag{38}$$

The same conditions as those in the insulator phase, the HP transformation, and the mean-field approximation are further employed to get $\hat{H}^S \simeq \hat{H}''$:

$$\begin{aligned} \hat{H}^S =& \frac{N(\epsilon - W)}{2} - NV_0 + \frac{N(1-m_c)^2G_0\sigma_0^2}{2} + \sum_{\boldsymbol{k}}\frac{\omega_{\boldsymbol{k}}}{4}\left(\tau_{\boldsymbol{k}}^2 + \tau_{\boldsymbol{k}}^{-2} - 2\right) + \sum_{\boldsymbol{k}}\omega_{\boldsymbol{k}}\tau_{\boldsymbol{k}}^2\hat{b}_{\boldsymbol{k}}^\dagger\hat{b}_{\boldsymbol{k}} + \sum_{\boldsymbol{k}}W\hat{a}_{\boldsymbol{k}}^\dagger\hat{a}_{\boldsymbol{k}} \\ &- (1-m)\left(\frac{\eta\epsilon}{W}\right)^2\sum_{\boldsymbol{k}}\left[\frac{g^2}{\omega_{\boldsymbol{k}}}\xi_{\boldsymbol{k}}(2-\xi_{\boldsymbol{k}}) - V_0\right](\hat{a}_{-\boldsymbol{k}}^\dagger + \hat{a}_{\boldsymbol{k}})(\hat{a}_{\boldsymbol{k}}^\dagger + \hat{a}_{-\boldsymbol{k}}), \\ &- \sqrt{(1-m)}\left(\frac{\eta\epsilon}{W}\right)\sum_{\boldsymbol{k}} g(1-\xi_{\boldsymbol{k}})\tau_{\boldsymbol{k}}(\hat{b}_{-\boldsymbol{k}}^\dagger + \hat{b}_{\boldsymbol{k}})(\hat{a}_{\boldsymbol{k}}^\dagger + \hat{a}_{-\boldsymbol{k}}) + \sqrt{(1-m)}\sum_{\boldsymbol{k}}\frac{\eta\epsilon g\xi_{\boldsymbol{k}}}{\omega_{\boldsymbol{k}}\tau_{\boldsymbol{k}}}(\hat{b}_{-\boldsymbol{k}}^\dagger - \hat{b}_{\boldsymbol{k}})(\hat{a}_{\boldsymbol{k}}^\dagger - \hat{a}_{-\boldsymbol{k}}), \end{aligned} \tag{39}$$

where the squeezing function $\tau_{\boldsymbol{k}}$ is given by

$$\tau_{\boldsymbol{k}}^2 = \sqrt{1 + \frac{4\eta^2\epsilon^2g^2\xi_{\boldsymbol{k}}^2}{W\omega_{\boldsymbol{k}}^3}}. \tag{40}$$

As we focus on the ground and low-lying excited states, we ignore all the cubic and quartic operators' interaction in deriving Eq. (39). Just as in the case of the insulating phase, we need another Bogoliubov transformation $\hat{S}_4$ to diagonalize $\hat{H}^S$, where

$$\hat{S}_4 = \frac{1}{2}\sum_{\boldsymbol{k}}\ln\left(\theta_{\boldsymbol{k}}^{-1}\right)(\hat{a}_{\boldsymbol{k}}\hat{a}_{-\boldsymbol{k}} - \hat{a}_{\boldsymbol{k}}^\dagger\hat{a}_{-\boldsymbol{k}}^\dagger) \tag{41}$$

with the parameter

$$\xi_k = \frac{\omega_k \tau_k^2}{\omega_k \tau_k^2 + W\theta_k^2}, \tag{42}$$

$$\theta_k^2 = \sqrt{1 - \frac{4(1-m)\eta^2\epsilon^2}{W^3}\left[\frac{g^2\xi_k(2-\xi_k)}{\omega_k} - V_0\right]}. \tag{43}$$

After the Bogoliubov transformation, we finally obtain the expression for the Hamiltonian as

$$e^{\hat{S}_4}\hat{H}^S e^{-\hat{S}_4} = E_g^S + \sum_k \omega_k \tau_k^2 \hat{b}_k^\dagger \hat{b}_k + \sum_k W\theta_k^2 \hat{a}_k^\dagger \hat{a}_k - \sum_k g_{Sk}(\hat{b}_k^\dagger \hat{a}_k + \hat{b}_k \hat{a}_k^\dagger) \tag{44}$$

with the effective coupling $g_{Sk} = 2\sqrt{(1-m)}g\eta\epsilon\tau_k(1-\xi_k)/(W\theta_k)$ between TLS and photon. The transformed Hamiltonian indeed provides a much better description than the RWA Hamiltonian. Using the linear transformation,

$$\hat{d}_{-k} = \cos\beta \hat{a}_k - \sin\beta \hat{b}_k, \tag{45}$$

$$\hat{d}_{+k} = \sin\beta \hat{a}_k + \cos\beta \hat{b}_k, \tag{46}$$

the system reduces to a diagonalized polariton model:

$$\hat{H} = E_g^S + \textstyle\sum_k E_S^{\pm}(\boldsymbol{k})\hat{d}_{\pm k}^\dagger \hat{d}_{\pm k},$$

where $\tan 2\beta = 2g_{Sk}/(\omega_k\tau_k^2 - \eta\epsilon\theta_k^2)$. This linear transformation reveals the composite nature of the polariton. The ground state of the polariton model is in the form of $|G_S\rangle = |\{\hat{d}_{\pm k}^\dagger \hat{d}_{\pm k} = 0\}\rangle$, and the corresponding ground-state energy of the delocalized superradiant phase is

$$E_g^S = \frac{N\left[\epsilon - 2W - 2V_0 + (1-m_c)^2 G_0\sigma_0^2\right]}{2} + \sum_k \frac{\omega_k}{4}\left(\tau_k^2 + \tau_k^{-2} - 2\right) + \sum_k \frac{W}{2}\theta_k^2. \tag{47}$$

From the ground state $|G_S\rangle$, we get the self-consistent equation

$$m = \langle G_S|e^{\hat{S}_4}\hat{a}_i^\dagger \hat{a}_i e^{-\hat{S}_4}|G_S\rangle = \frac{1}{4N}\sum_k \left(\theta_k^{-2} + \theta_k^2 - 2\right). \tag{48}$$

The dispersion relations of the two branches of polaritonic excitations in the delocalized superradiant phase are

$$E_S^{\pm}(\boldsymbol{k}) = \frac{1}{2}\left(W\theta_k^2 + \omega_k\tau_k^2\right) \pm \frac{1}{2}\sqrt{\left(W\theta_k^2 - \omega_k\tau_k^2\right)^2 + 4g_{Sk}^2}. \tag{49}$$

The stability of the delocalized superradiant phase requires the energy cost for the polariton excitations. Thus, the lower branch polariton excitation energy $E_S^-(\boldsymbol{k})$ needs to be positive, and the following equation should be satisfied:

$$W\theta_{\boldsymbol{0}}^2\omega_{\boldsymbol{0}}\tau_{\boldsymbol{0}}^2 \geqslant g_{S\boldsymbol{0}}^2 \Rightarrow 2(1-m)G_{\boldsymbol{0}}\left(\frac{\eta\epsilon}{W}\right)^2 \leqslant W. \tag{50}$$

By the relation $2(1-m_c)G_0 = W$ and $1 - m_c \leqslant 1 - m$, the condition for the presence of the stable delocalized superradiant phase can be written as

$$2(1-m)G_0 \geqslant \eta\epsilon, \tag{51}$$

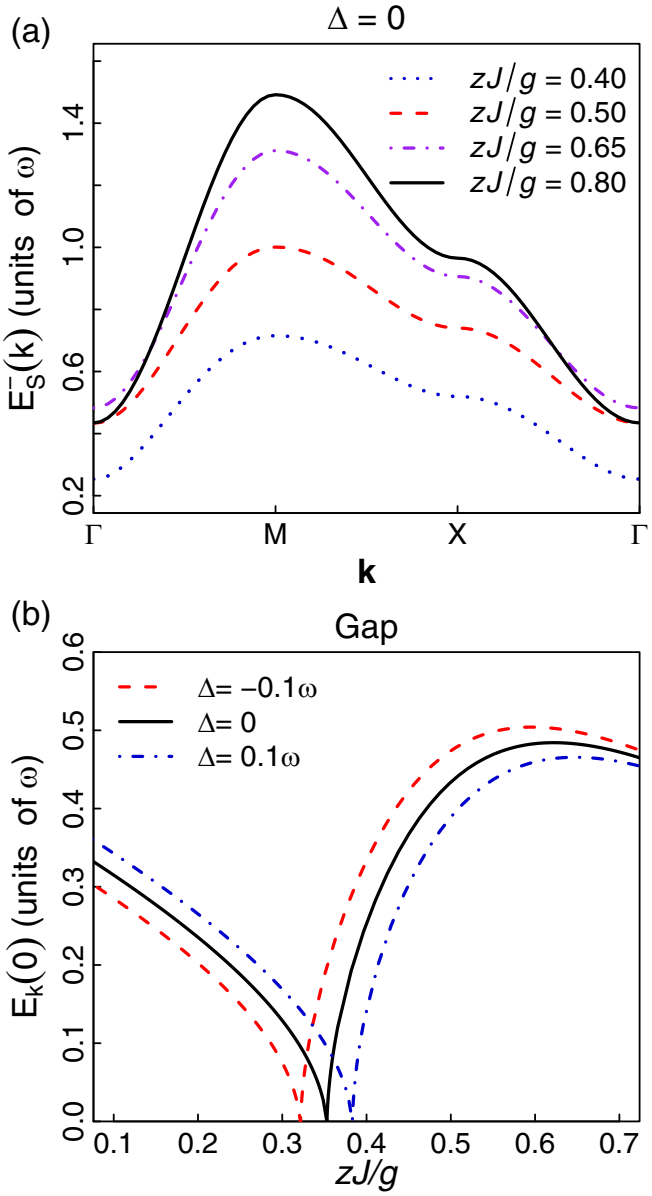

FIG. 7. (a) The dispersion relation of the low-branch polaritonic excitations $E^-(\boldsymbol{k})$ for the two-dimensional square lattice RLM at $\omega = 1.5g$ in the delocalized superradiant phase. (b) The gap of the excitation as a function of the hopping strength zJ. Energies are in the units of ω.

which is in accordance with the results in the insulating phase.

Around the critical hopping strength J_c, the behaviors of the low branch polariton excitations $E_S^-(\boldsymbol{k})$ in the delocalized superradiant phase are also plotted in Figs. 2(d)–2(f). For the negative detuning case $\Delta = -0.1\omega$, $E_I^-(\boldsymbol{0})$ also has a positive gap at $zJ = 0.376(> zJ_c)$, as plotted with the blue dashed line in Fig. 2(d). For the resonant case $\Delta = 0$, the $\boldsymbol{k} = 0$ gap opens again at $zJ/g = 0.380(> zJ_c)$ in Fig. 2(e) (blue dashed line). For the positive detuning case $\Delta = 0.1\omega$, $E_I^-(\boldsymbol{0})$ exists a gap at $zJ = 0.430(> zJ_c)$, in Fig. 2(f) (blue dashed line).

The spectra of the gapped polariton excitations in the delocalized superradiant phase are plotted in Fig. 7(a) at $\omega = 1.5$ for the resonant case $\Delta = 0$, which is quite different from the gapless excitation in the JCLM [22–24,28]. In the JCLM,

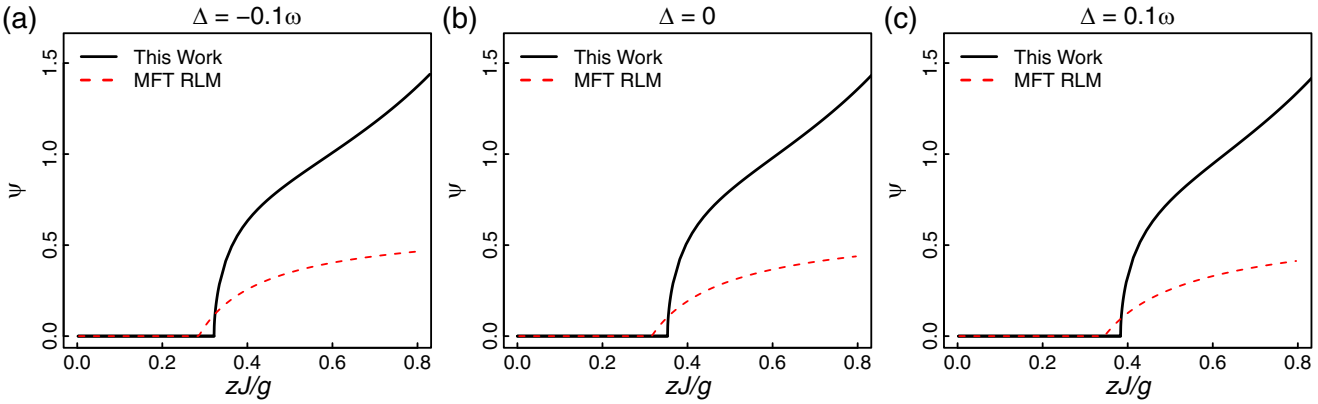

FIG. 8. The order parameter as a function of the hopping strength zJ at $\omega = 1.5g$: (a) the negative detuning case $\Delta = -0.1\omega$; (b) the resonant case $\Delta = 0$; (c) the positive detuning case $\Delta = 0.1\omega$.

the system has continuous $U(1)$ symmetry, and the Goldstone theorem requires gapless excitation to restore the symmetry. While the CRC terms break continuous symmetry into discrete Z_2 symmetry, the Goldstone theorem does not apply here. To overview the property of the excitations, the $\boldsymbol{k} = 0$ gap of the polaritonic excitations as a function of the hopping strength zJ is plotted in Fig. 7(b). The polaritonic excitations have a positive gap in both the insulator and delocalized superradiant phase, but the gap vanishes at the phase transition point.

Different from the Mott insulator state, where each site has a fixed number of photons, the photon number per site is not fixed in the delocalized superradiant phase due to the hopping coupling. Thus, the order parameter is calculated as the expectation of the photonic annihilation operator in the ground state, which is given by

$$\begin{aligned}\psi &= \langle G_S|e^{\hat{S}_4}\hat{U}^\dagger e^{\hat{R}}e^{\hat{S}_2}e^{\hat{S}_1}\hat{b}_i e^{-\hat{S}_1}e^{-\hat{S}_2}e^{-\hat{R}}\hat{U}\,e^{-\hat{S}_4}|G_S\rangle \\ &= \frac{g\sigma_0\xi_{\mathbf{0}}}{\omega_{\mathbf{0}}}(m_c - 2m) + \frac{g\sigma_0}{\omega_{\mathbf{0}}}. \end{aligned} \tag{52}$$

The order parameter growing from zero to a nonvanishing expectation is shown in Fig. 8 for the negative detuning case $\Delta = -0.1\omega$, the resonant case $\Delta = 0$, and the positive detuning case $\Delta = 0.1\omega$ at $\omega = 1.5g$. With the increasing of the hopping strength, more polaritons tend to condense on the ground state, which indicates the stronger order parameter. From Eq. (52), our results suggest that the order parameter $\psi \propto \frac{g}{\omega_0}$, which increases more quickly than the MFT results.

VI. CONCLUSION

In summary, we use the unitary transformation method to study the physics of the RLM. Phase diagrams and polaritonic excitation spectra have been explored. The CRC terms, which are usually neglected in weak-coupling cases, have remarkable impacts on the ground state and low-lying excited states and consequently change the nature of the phase transition. With the increasing of the hopping strength J, the RLM undergoes quantum phase transition from insulator to delocalized superradiant phase. In the Mott insulator phase, the intrasite repulsion leads to the polariton localizing on each site and the ground state being the net excitation per site. Gradually increasing the hopping strength to the critical point J_c, the ground state becomes no longer stable, and Bose-Einstein condensation emerges. Above the critical point, the polariton delocalizes across the lattice, and the photon coherence has a nonvanishing expectation. From the stability of the ground state both in the insulator and delocalized superradiant phase, we obtain the analytical expression for the boundary of the phase transition. The CRC terms break the conservation polariton number, leading to the absence of Mott lobes in the RLM phase diagram. The results also show that the larger detuning favors the disorder insulator phase, and the system needs the stronger hopping coupling J_c to reach the long-range order delocalized superradiant phase.

In comparison with the QTFI and MFT, the advantages of the unitary transformation method are obvious. The MFT requires symmetry breaking $\psi(\hat{b}_i^\dagger + \hat{b}_i)$ and reduces the Hamiltonian to the single-site model, which gives the N degeneracy excitation energy. The MFT neglects the long-range correlation between the different sites and breaks down in the strong hopping case. The effective QTFI Hamiltonian is obtained in the photon vacuum state and is valid in the strong-coupling case. In our method, through the Bogoliubov transformation, the system maps to the polariton model. The effects of the CRC terms are explored by renormalized quantities such as g_{Ik}, $\epsilon\eta\rho_{\boldsymbol{k}}^2$, and $\omega_k\tau_{\boldsymbol{k}}$. Due to the coupling between the photons and the TLSs, the composite nature of the polariton is captured. The hybridized polaritonic states in the RLM are different from the phases obtained from the effective QTFI Hamiltonian, which is just the atomic excitations. The spectral properties of the polaritonic excitation are further evaluated. In both the insulator phase and delocalized superradiant phase, the RLM has gapped polaritonic excitation, which ensures the stability of the ground state. This gap closes at the critical point, which indicates that the Z_2 symmetry is broken and the phase transition occurs. As the introduced photon-dressing parameter η includes the infinite order of g, our results on the ground and low-lying excited states work well for both the weak-coupling and strong-coupling case.

ACKNOWLEDGMENTS

This work is supported by National Natural Science Foundation of China Grants No. 11947231, No. 11874260, and No. 11774226.

[1] I. I. Rabi, Phys. Rev. **49**, 324 (1936).
[2] A. Wallraff, D. I. Schuster, A. Blais, L. Frunzio, R. S. Huang, J. Majer, S. Kumar, S. M. Girvin, and R. J. Schoelkopf, Nature (London) **431**, 162 (2004).
[3] P. Forn-Díaz, J. Lisenfeld, D. Marcos, J. J. García-Ripoll, E. Solano, C. J. P. M. Harmans, and J. E. Mooij, Phys. Rev. Lett. **105**, 237001 (2010).
[4] E. Jaynes and F. Cummings, Proc. IEEE **51**, 89 (1963).
[5] M. Brune, F. Schmidt-Kaler, A. Maali, J. Dreyer, E. Hagley, J. M. Raimond, and S. Haroche, Phys. Rev. Lett. **76**, 1800 (1996).
[6] P. Forn-Díaz, L. Lamata, E. Rico, J. Kono, and E. Solano, Rev. Mod. Phys. **91**, 025005 (2019).
[7] A. Frisk Kockum, A. Miranowicz, S. De Liberato, S. Savasta, and F. Nori, Nat. Rev. Phys. **1**, 19 (2019).
[8] A. Crespi, S. Longhi, and R. Osellame, Phys. Rev. Lett. **108**, 163601 (2012).
[9] J. Casanova, G. Romero, I. Lizuain, J. J. García-Ripoll, and E. Solano, Phys. Rev. Lett. **105**, 263603 (2010).
[10] Q. Mei, B. Li, Y. Wu, M. Cai, Y. Wang, L. Yao, Z. Zhou, and L. Duan, arXiv:2110.03227.
[11] J. M. Raimond, M. Brune, and S. Haroche, Rev. Mod. Phys. **73**, 565 (2001).
[12] A. Zeilinger, Rev. Mod. Phys. **71**, S288 (1999).
[13] A. A. Houck, H. E. Türeci, and J. Koch, Nat. Phys. **8**, 292 (2012).
[14] S. Schmidt and J. Koch, Ann. Phys. (NY) **525**, 395 (2013).
[15] M. J. Hartmann, F. G. Brandão, and M. B. Plenio, Nat. Phys. **2**, 849 (2006).
[16] A. D. Greentree, C. Tahan, J. H. Cole, and L. C. L. Hollenberg, Nat. Phys. **2**, 856 (2006).
[17] I. Bloch, J. Dalibard, and S. Nascimbène, Nat. Phys. **8**, 267 (2012).
[18] D. Ballester, G. Romero, J. J. García-Ripoll, F. Deppe, and E. Solano, Phys. Rev. X **2**, 021007(2012).
[19] D. Lv, S. An, Z. Liu, J.-N. Zhang, J. S. Pedernales, L. Lamata, E. Solano, and K. Kim, Phys. Rev. X **8**, 021027 (2018).
[20] D. G. Angelakis, M. F. Santos, and S. Bose, Phys. Rev. A **76**, 031805(R) (2007).
[21] M. Hartmann, F. Brandão, and M. Plenio, Laser Photonics Rev. **2**, 527 (2008).
[22] D. Rossini and R. Fazio, Phys. Rev. Lett. **99**, 186401 (2007).
[23] S. Schmidt and G. Blatter, Phys. Rev. Lett. **103**, 086403 (2009).
[24] S. Schmidt and G. Blatter, Phys. Rev. Lett. **104**, 216402 (2010).
[25] A. Imamoğlu, H. Schmidt, G. Woods, and M. Deutsch, Phys. Rev. Lett. **79**, 1467 (1997).
[26] K. M. Birnbaum, A. Boca, R. Miller, A. D. Boozer, T. E. Northup, and H. J. Kimble, Nature (London) **436**, 87 (2005).
[27] J. Koch and K. Le Hur, Phys. Rev. A **80**, 023811 (2009).
[28] M. Aichhorn, M. Hohenadler, C. Tahan, and P. B. Littlewood, Phys. Rev. Lett. **100**, 216401 (2008).
[29] M. Knap, E. Arrigoni, and W. Von Der Linden, Phys. Rev. B **81**, 104303 (2010).
[30] H. Zheng and Y. Takada, Phys. Rev. A **84**, 043819 (2011).
[31] M. Schiró, M. Bordyuh, B. Öztop, and H. E. Türeci, Phys. Rev. Lett. **109**, 053601 (2012).
[32] M. Schiró, M. Bordyuh, B. Öztop, and H. E. Türeci, J. Phys. B **46**, 224021 (2013).
[33] S. Cui, F. Hébert, B. Grémaud, V. G. Rousseau, W. Guo, and G. G. Batrouni, Phys. Rev. A **100**, 033608 (2019).
[34] B. Kumar and S. Jalal, Phys. Rev. A **88**, 011802(R) (2013).
[35] T. Flottat, F. Hébert, V. G. Rousseau, and G. G. Batrouni, Eur. Phys. J. D **70**, 213 (2016).
[36] T. Holstein and H. Primakoff, Phys. Rev. **58**, 1098 (1940).
[37] D. Braak, Phys. Rev. Lett. **107**, 100401 (2011).
[38] E. K. Irish, Phys. Rev. Lett. **99**, 173601 (2007).
[39] Q.-H. Chen, C. Wang, S. He, T. Liu, and K.-L. Wang, Phys. Rev. A **86**, 023822 (2012).
[40] E. Lieb, T. Schultz, and D. Mattis, Ann. Phys. (NY) **16**, 407 (1961).
[41] P. Pfeuty, Ann. Phys. (NY) **57**, 79 (1970).
[42] M. Henkel, J. Phys. A **20**, 3969 (1987).
[43] C.-J. Huang, L. Liu, Y. Jiang, and Y. Deng, Phys. Rev. B **102**, 094101 (2020).
[44] E. K. Irish, C. D. Ogden, and M. S. Kim, Phys. Rev. A **77**, 033801 (2008).